NPL REPORT CBTLM 7

Production, measurement and analysis of sinusoidal artefacts for calibration of surface texture measuring instruments

Richard K Leach, Ian Garbutt, Peter Harris,
Maurice Cox

January 2001

Production, measurement and analysis of sinusoidal reference artefacts for calibration of surface texture measuring instruments

Richard K Leach*, Ian Garbutt*, Peter Harris** & Maurice Cox**
*Centre for Basic, Thermal & Length Metrology
**Centre for Mathematics & Scientific Computing
National Physical Laboratory
Queens Road
Teddington
Middlesex
United Kingdom
TW11 0LW

Abstract

As part of a collaborative project, gratings with sinusoidal profiles and with periods in the range of 0.8 to 25 μm have been developed at the National Physical Laboratory (NPL). The gratings are formed in photoresist-coated substrates by exposing them to an optical interference pattern. The photoresist gratings are then replicated into electroformed nickel. The gratings are measured using the NanoSurf IV instrument and the measurement data are analysed using mathematical algorithms developed at NPL to extract the period and amplitude.

ISSN 1369 - 6777

National Physical Laboratory
Queens Road, Teddington, Middlesex, United Kingdom, TW11 0LW

Approved on behalf of the Managing Director
by Dr David Robinson, Head of the Centre for Basic, Thermal & Length Metrology

CONTENTS

FIGURE LEGENDS

1. INTRODUCTION

This report describes the work carried out at NPL as part of the EC project SMT 4 – CT97 – 2176 "Calibration standards for surface topography measuring systems down to nanometric range" that ran for 38 months and finished in December 2000. The project was concerned with developing standards, including their production methods and calibration procedures. The other participants in the projects were: Technische Universität Chemnitz (Germany), University of Warwick (UK), Bayer AG (Germany), Stiftung Institut für Werkstofftechnik (Germany), Danmarks Tekniske Universitet (Denmark), Rubert + Co. (UK) and FZM GmbH (Germany).

The task of NPL was to produce surfaces with sinusoidal profiles (referred to as Type C1 artefacts in ISO 5436: 1999) for use in calibrating surface texture measuring instruments. The method used by NPL was to produce master gratings in photoresist by recording the interference fringes formed at the intersection of two coherent laser beams. These master gratings were then replicated so that they could be used as robust artefacts that could be measured using contacting techniques.

2. HOLOGRAPHIC GRATING GENERATION

The sinusoidally modulated surfaces are produced at NPL using the interferometer in shown schematically in figure 1.

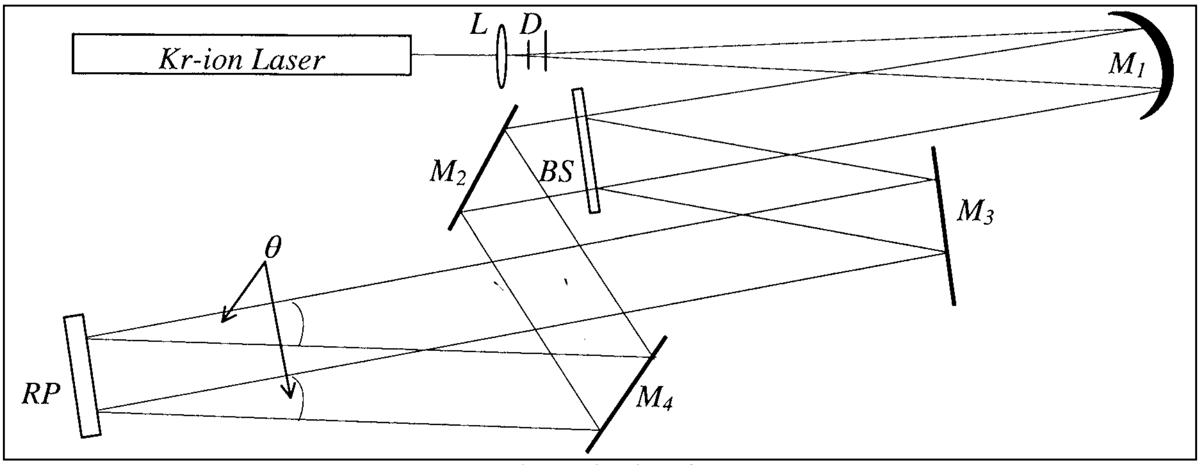

Figure 1 The grating interferometer

The 413 nm line from a Kr-ion laser is used as the coherent light source. A short focal length lens *L* expands the beam. Diffuser *D* is placed in the expanding beam to scramble its spatial coherence and vary the characteristics of the laser speckle associated with coherent light source. Mirror M_1 is situated at a distance equal to the sum of its focal length and that of *L*, collimating the expanded beam. The beam splitter *BS* then divides the beam. Mirrors M_2, M_3 and M_4 are positioned such that the two resulting beam paths are of the same length when recombined at the recording plane *RP* and are bisected by a pre-determined angle θ. The interference pattern at *RP* is a set of parallel fringes whose intensity varies sinusoidally in a certain direction.

The angle θ determines the period of the grating that is given by the grating equation

$$n\lambda = 2d\sin\theta \qquad (1)$$

where n is the order of diffraction (which is unity in this case), λ is the wavelength of the light, θ is the beam bisecting angle and d is the fringe spacing or grating period.

The fringes are recorded in photoresist and with careful control/selection of the exposure and development criteria, the developed resist contains a pattern with the same period, and a modulation proportional, to the intensity profile of the interference fringes. These profiled resist surfaces form masters for the later production of the robust replica sinusoids.

The photoresist is coated in an even layer about 1 μm thick over the surface of an optically worked glass substrate using a commercial centrifugal spin coater. The thickness of the layer is determined by the spin speed, spin duration and the viscosity of the resist used. For the purposes of this project a relatively low viscosity resist was chosen. Lower viscosity resists have the advantage of being less prone to suspended particle contamination, one potential cause of poor quality micro textured surfaces. Any airborne particulate contamination of the photoresist before spinning or subsequent drying will give rise to a poor quality resist layer. For this reason, all of the photoresist spinning, and some of the final substrate cleaning, is carried out in class 100 clean room conditions with full vertical laminar airflow.

It is essential that the worked surfaces of the substrates are extremely clean prior to spinning. Freshly worked substrates are cleaned using a 20:1 Teepol solution. After drying in a stream of filtered and compressed air they are further cleaned with iso-2-propanol. Due to the repetitive nature of the process, substrates may be coated with resist more than once before reworking is necessary. In these cases the worked surface is first stripped of old photoresist using SLR grade Acetone, then cleaned using an abrasive commercial substrate cleaner to ensure the complete removal of any stubborn or insoluble resist films. The substrates are given a final clean using methenol under clean conditions immediately prior to spinning the resist.

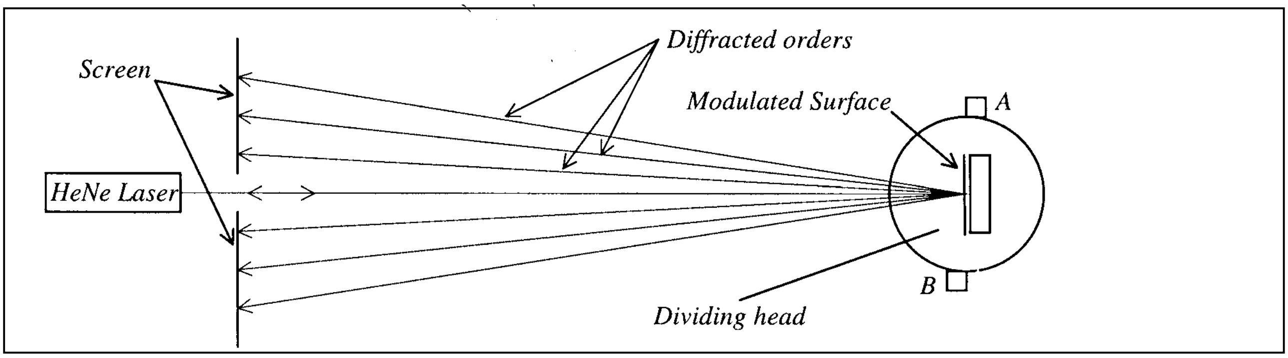

Figure 2. The dividing head diffractometer

To obtain a surface with the required period, the angle θ is calculated using equation 1. The interferometer mirrors M_3 and M_4 are located with respect to *RP* to a first approximation by means of a rotary table with an angular Vernier scale. An exposure is made and the period of the resulting surface is determined using the dividing head diffractometer shown in figure 2. This measures the angle of a beam of monochromatic light diffracted by the modulated surface. The scale is read at *A* and *B*. The period of the surface can then be calculated, once again using equation 1. A correction is applied to *RP* and the necessary adjustments made to M_3 and M_4. Another exposure is made and the resulting surface measured, this process is repeated several times until the required period is achieved.

The modulation depth of the surface intensity profile is dependent on exposure time, beam intensity, spatial coherence of the expanded beam and photoresist development conditions. The exposure time and beam intensity are the primary controlling factors. Longer exposures will penetrate deeper in to the volume of the resist layer and remove more of the exposed resist. If the exposure and or the development are excessive the resulting surface will resemble **c.** shown in figure 3. The opposite is true if the same factors are insufficient resulting in a profile resembling **a.**

A compromise has to be reached where a sinusoidal profile similar to the one shown in **b**. is achieved.
The beam intensity can also be varied - at lower intensities the exposure time has to be increased to achieve a comparable modulation depth. Longer exposure times give better control of the exposure repeatability.

The typical development times for concentrated Shipley microposit developer are of the order of seconds, diluting the developer with high purity de-ionised water increases these times, giving better control of the development conditions.

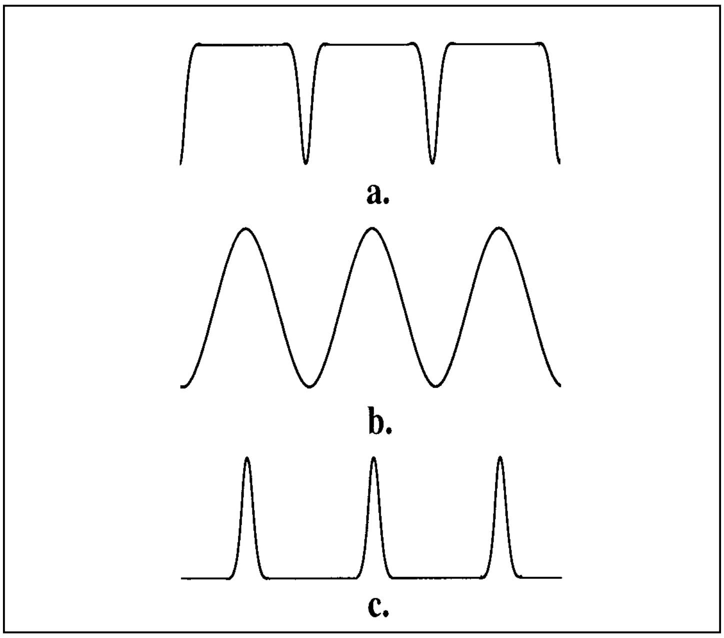

Figure 3. Typical photoresist surface profiles

The extent to which the diffuser *D*, shown in figure 1, scrambles the spatial coherence of the expanded beam, has an effect on the modulation depth. The more the beam is scrambled the lower the modulation. However, too little scrambling has adverse effects on the quality of the projected wave fronts, which cannot be tolerated.

3. EARLY REPLICATION EXPERIMENTS

The early gratings occupied an area approximately 30 mm by 35 mm on 6 mm thick glass substrates 100 mm square. The gratings were produced with periods of 0.8, 2.5 and 8 µm with depths between 0.15 and 0.5 µm. A selection of gratings were replicated in silicon elastomer and then copied by casting in epoxy resin onto glass substrates. Rubert + Co. was provided with samples for trials with electroless nickel plating and other means of generating electroforms from insulating master gratings. TUC and DTU also received copies of the gratings for measurements. Note that at this point in the project NPL was not in a position to make traceable measurements of the samples. The measurements at TUC showed that the samples were useful for testing the typical filters used on surface texture measuring instruments and the influence of the finite geometry of a stylus.

The initial replication experiments showed that the processes were not robust enough to get good quality nickel copies of the masters and that the cast and plastic copies exhibited a high degree of form and waviness error that could not be tolerated.

4. ELECTROFORMING USING NICKEL

Opsec plc were chosen to grow the nickel electroformed shims from the NPL photoresist master surfaces.

The nickel electroforming process is in three parts:

i. The photoresist master is coated with an opaque evaporated silver-seeding layer. This is then placed in the electrolyte bath where the electroforming takes place under controlled conditions. After a calculated period of time, the masters are removed from the tank and the negative (-ve) nickel replica is separated from the master. This -ve electroform is known as a -ve sub-master.

ii. The -ve sub-master is then treated in the same way as the photoresist master to produce the +ve sub-master.

iii. The sub-masters can be used to produce numerous +ve and –ve replica nickel shims.

One inherent problem with the production of electroformed nickel is surface flatness. There are two factors, which have been identified as contributors to the curvature of electroformed surfaces. The biggest contributor to the loss of shim flatness is the parting of the electroform from its master. The shim has a tendency to peel away from the master rather than snap apart thus imparting curvature to the shim. The other factor concerns the concave back surface of the shim; this is a result of the accelerated nickel growth at outer edges of the master during the process.

Growing thicker shims was a possible solution to the parting problem as this would give the shim more rigidity and less of a tendency to peel and deform during parting. Unfortunately the thicker shims magnified the back surface curvature. This causes stresses to build up within the shim, which try (and some times succeeded) in prematurely pulling the shim away from its master while still in the growing tank, leaving the shim with a convex or buckled surface.

Several new techniques were applied to these problems. These included building up the size of the photoresist master to an effective 150 x 150 mm substrate size. It was hoped that the larger surface area would tend to minimise the shim back surface curvature over the actual master substrate area. It was later found that the master shim required an insulating tape break to be fabricated before the growth of the shim to allow the removal of the 100 x 100 mm shims from the oversized artefact. Without the break the resulting oversize shim was saucer shaped and could not be guillotined to size. Variations were also made to the magnitude of the electric current density used to grow the shims - increasing the current density speeds up the process and *vice versa*. The other growth parameter to be varied was the growing temperature (usually 55 ^{o}C). The different materials involved in the electroforming process have differing coefficients of thermal expansion, which may in part be responsible for the premature parting of the shims from the masters.

The above techniques did improve the overall flatness of the finished shims but further improvement in this area would be beneficial to future work.

5. MEASUREMENT USING NANOSURF IV

The gratings were measured using the NanoSurf IV – an instrument that uses optical interferometry to measure the position of a stylus tip as it traces over the surface topography (Leach 2000). The uncertainty analysis of NanoSurf IV has been calculated according to the PD 6461 Part 3 (1995) (*GUM*) and is presented elsewhere (Leach 1999). The combined standard uncertainty of measurements in the x and z axes at 95% confidence is ± 1.3 nm. NanoSurf IV is linked to the realisation of the metre via the calibrated frequency of its laser source.

6. THE ANALISYS SCHEME

The measured data consists of the locus of the stylus-tip centre as discretised by an analogue-to-digital converter. For sufficiently small stylus-tip radii, *i.e.*, less than the smallest radius of curvature of the surface profile, this locus represents a meaningful *offset* curve. An offset curve is a curve that is a constant distance from the surface profile, where distance is measured orthogonally to the profile. In particular, the amplitude of the offset curve for a periodic function will be equal to that of the periodic function itself in the case where the above curvature condition applies. This statement is true because the stylus tip will make physical contact with the surface profile at the peaks and troughs of the latter in this case. Thus, an estimate of the amplitude of the surface profile curve is given by that of the offset curve. Moreover, an estimate of the period of the fundamental frequency can similarly be determined from the offset curve. The departure from a pure sinusoid cannot be determined directly, however, from such departure for the offset curve, since the offset curve for a pure sinusoid is not a pure sinusoid. This part of the study is concerned with the information about the variation in period and amplitude along a measurement trace that can be extracted from the measurements of the offset curve without knowledge of the stylus other than the above curvature condition.

A method of estimation, which is essentially *non-parametric* (*i.e.* one derived from the data without the use of a regression model), of the manner in which

(a) the period, and
(b) the amplitude,

varies along a measurement trace is used. This involves locating the zero-crossing points of the measurement trace as represented by the data and using the distances between every other such zero as values of the local period. The maximum and minimum values of the measurement trace between every other such zero provides estimates of the local peak and trough values. The set of values for the local period describes the variation of period along the measurement trace, and is summarised using the arithmetic mean and standard deviation statistics. Similarly for the sets of local peak and local trough values.

Due the presence of local maxima and minima along a measurement trace resulting from the effect of measurement error, it can happen that estimates of the local period that are very large or small compared to the nominal value of the period can be determined. A simple test, based on excluding values that differ from the nominal value by an amount that exceeds a specified tolerance, is used to exclude such estimates.

The method of estimation consists of the following steps:

Step 1: The effect of misalignment of the measured artefact with respect to the measurement instrument is removed from the raw data by subtracting the values of a polynomial function determined as the least-squares best-fit polynomial to the raw data.

Step 2: For the resulting set of corrected data points $\{(x_i, z_i)\}$, and for a number of choices of h lying between the minimum and maximum values of z_i:

> *Step 2a*: The subset of values of i such that either (a) $z_i = h$ and $z_{i+1} = h$ or (b) $z_i = h$ and $z_{i+1} = h$ is determined. These values of i therefore have the property that (in the absence of error) the measurement trace $z = f(x)$ represented by the data points crosses the (constant) function $z = h$ between x_i and x_{i+1}, i.e., the function $f(x) - h$ takes the value zero at some point in this interval.
>
> *Step 2b*: Inverse linear interpolation is used to identify the zero-crossing points for $f(x) - h$ in these intervals. Note that the zero-crossing points corresponding to (a) in Step 2a lie on *rising* parts of the measurement trace, and those corresponding to (b) lie on *falling* parts of the measurement trace.
>
> *Step 2c*: The distances between neighbouring zeros on rising parts of the measurement trace and those between zeros on falling parts of the measurement trace are taken as estimates of the *local pitch* of the measured artefact in the neighbourhoods of the zero crossings.
>
> *Step 2d*: The maximum and minimum values of the corrected data lying between successive zeros lying on (say) rising parts of the measurement trace are taken as estimates, respectively, of the *local peak* and *local trough*.

7. FIRST GENERATION SINUSOIDS

The results of the measurements and analyses are presented below for one positive and one negative copy of each of the nominal periods. Data set names with an *n* in them correspond to negative and *p* to positive. Note that when a value is not given for the mean or standard deviation of a local peak or a local trough value, it is because there is so much variation that these statistics are essentially meaningless. All the ordinate values are in nanometres, but those of the abscissae are arbitrary units.

0.8 μm period grating

Data set	*Local Period*		*Local Peak*		*Local Trough*	
	Mean (μm)	Standard Deviation (μm)	Mean (nm)	Standard Deviation (nm)	Mean (nm)	Standard Deviation (nm)
dgnr1	0.827	0.035	–	–	–	–
dgpf1	0.811	0.043	–	–	–	–

In the table above, the mean and standard deviation of the estimates for each grating are given. Figures 4 and 5 show the raw data (after a misalignment correction) with estimates of the peak and trough positions marked.

The non-parametric analysis of the traces is more difficult for this period size compared with the 2.5 µm and 8 µm period gratings considered below. Numerous "spurious" values for local period were obtained. The computed statistics for the variation in local period across each grating are consequently dependent on the scheme used to exclude these spurious values (see Section 6). Similarly, numerous spurious peaks and troughs are also identified (see Figures 4 and 5) and statistics relating to local peak and trough values are not reliable and are not presented in the above table.

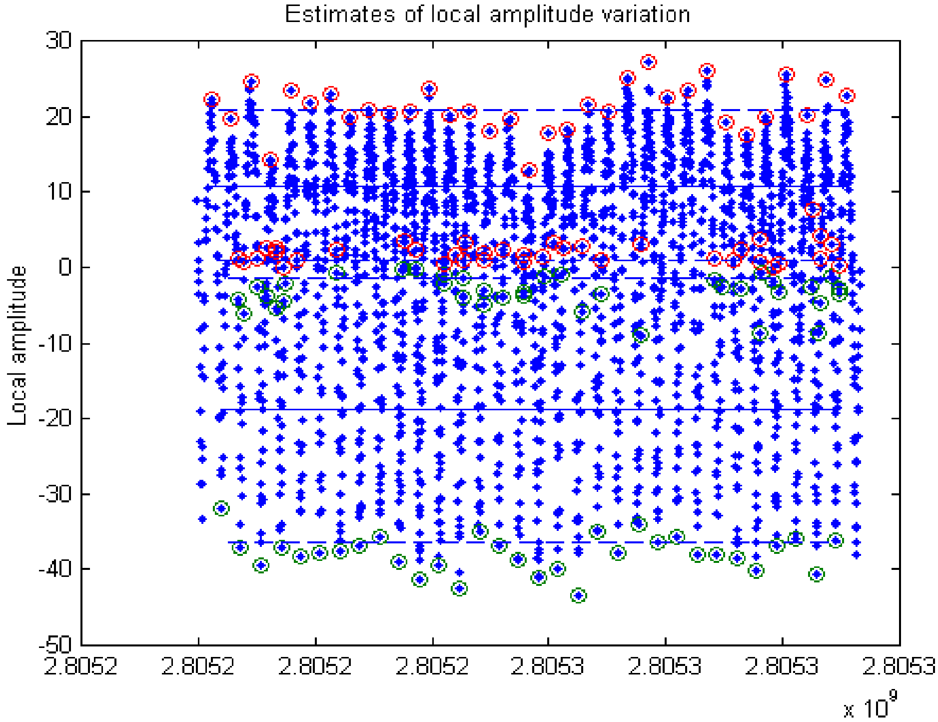

Figure 4. Positions of peaks and troughs (circles), together with the mean and mean ± one standard deviation value (horizontal lines) for data set **dgnr1** (0.8 µm period grating)

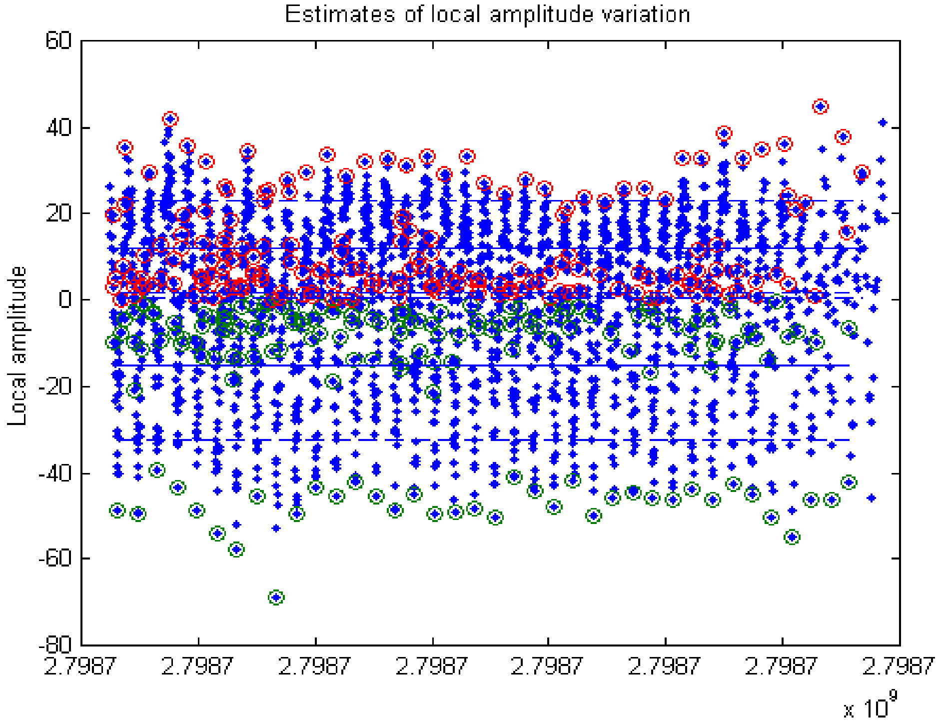

Figure 5. Positions of peaks and troughs (circles), together with the mean and mean ± one standard deviation value (horizontal lines) for data set **dgpf1** (0.8 µm period grating)

2.5 μm period grating

Data set	*Local Period*		*Local Peak*		*Local Trough*	
	Mean (μm)	Standard Deviation (μm)	Mean (nm)	Standard Deviation (nm)	Mean (nm)	Standard Deviation (nm)
bgnf1	2.531	0.057	–254.757	10.997	134.508	13.125
bgpr1	2.534	0.045	–287.810	11.605	175.474	14.037

Figures 6 and 7 show the results of the analysis of the 2.5 μm period gratings, and the table above gives the mean and standard deviation of the estimates of local period, local peak value and local trough value for the two gratings. Unlike the 0.8 μm period gratings considered above, the local peaks and troughs are correctly identified by the analysis scheme.

Note that (a) the values of the mean local period for the two data sets are very close and exceed the nominal 2.5 μm value, and (b) the traces represented by the two data sets have markedly different peak-to-valley values.

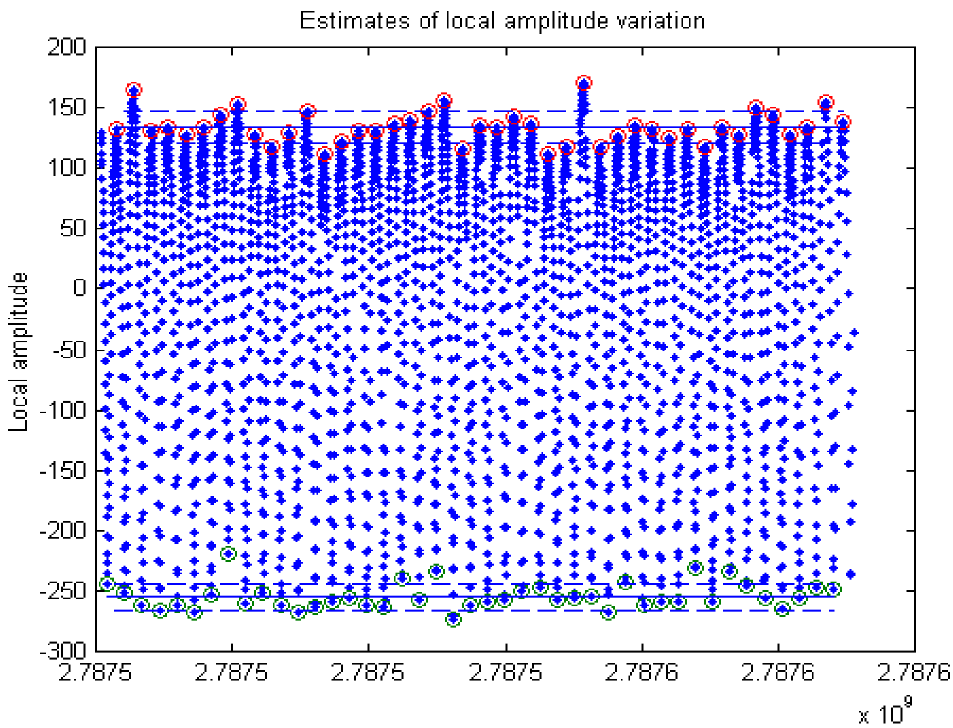

Figure 6. Positions of peaks and troughs (circles), together with the mean and mean ± one standard deviation value (horizontal lines) for data set **bgnf1** (2.5 μm period grating)

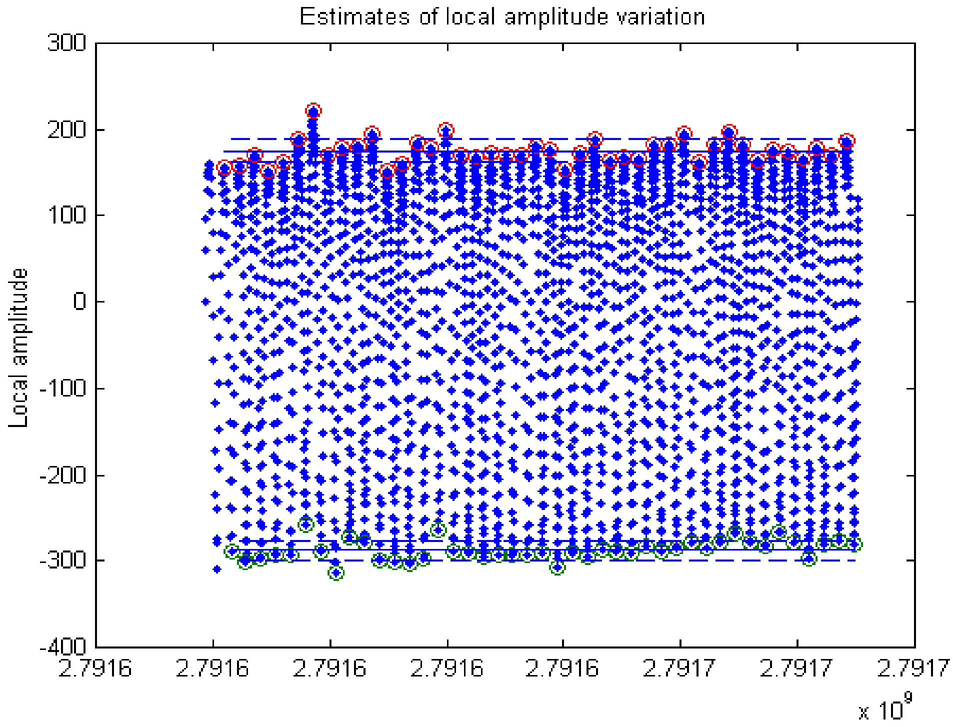

Figure 7. Positions of peaks and troughs (circles), together with the mean and mean ± one standard deviation value (horizontal lines) for data set **bgpr1** (2.5 μm period grating)

8 μm period grating

Data set	***Local Period***		***Local Peak***		***Local Trough***	
	Mean (μm)	Standard Deviation (μm)	Mean (nm)	Standard Deviation (nm)	Mean (nm)	Standard Deviation (nm)
a1nf1	7.925	0.109	−219.900	16.516	243.293	21.117
a1pf14	7.927	0.107	−206.437	15.499	212.320	14.213

Figures 8 and 9 show the results of the analysis of the 8 μm period gratings, and the table above gives the mean and standard deviation of the estimates of local period, local peak value and local trough value for the two gratings. As for the 2.5 μm period gratings considered above, the local peaks and troughs are correctly identified by the analysis scheme.

Note that (a) the values of the mean local period for the two data sets are very close and are smaller than the nominal 8 μm value, and (b) there is better consistency in the different peak-to-valley values for the traces than was obtained for the 2.5 μm period grating.

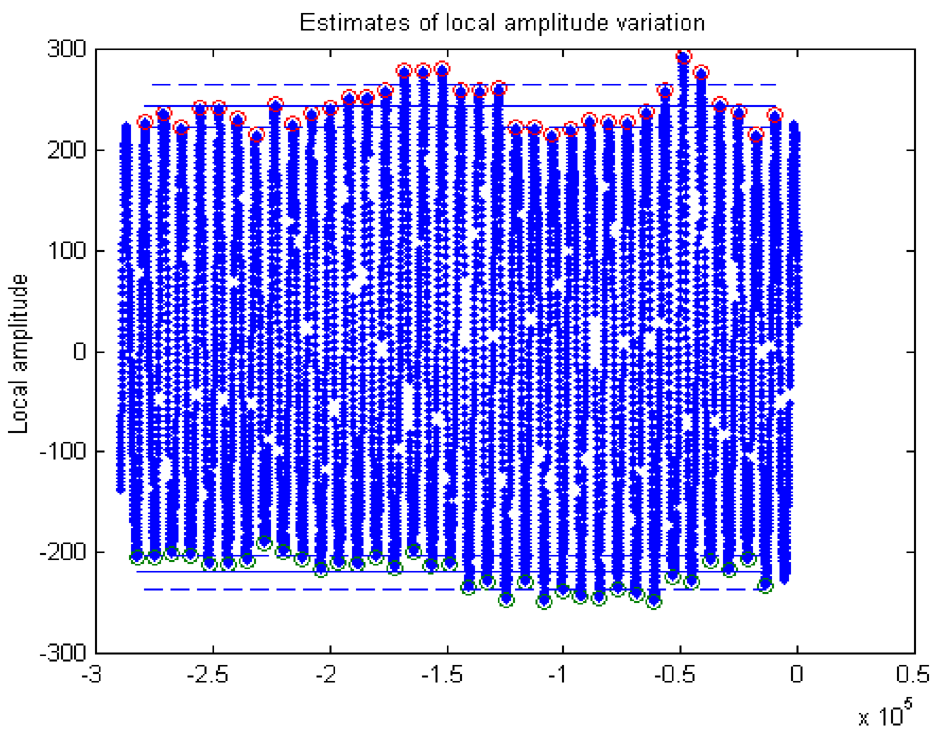

Figure 8. Positions of peaks and troughs (circles), together with the mean and mean ± one standard deviation value (horizontal lines) for data set **a1nf1** (8 µm period grating)

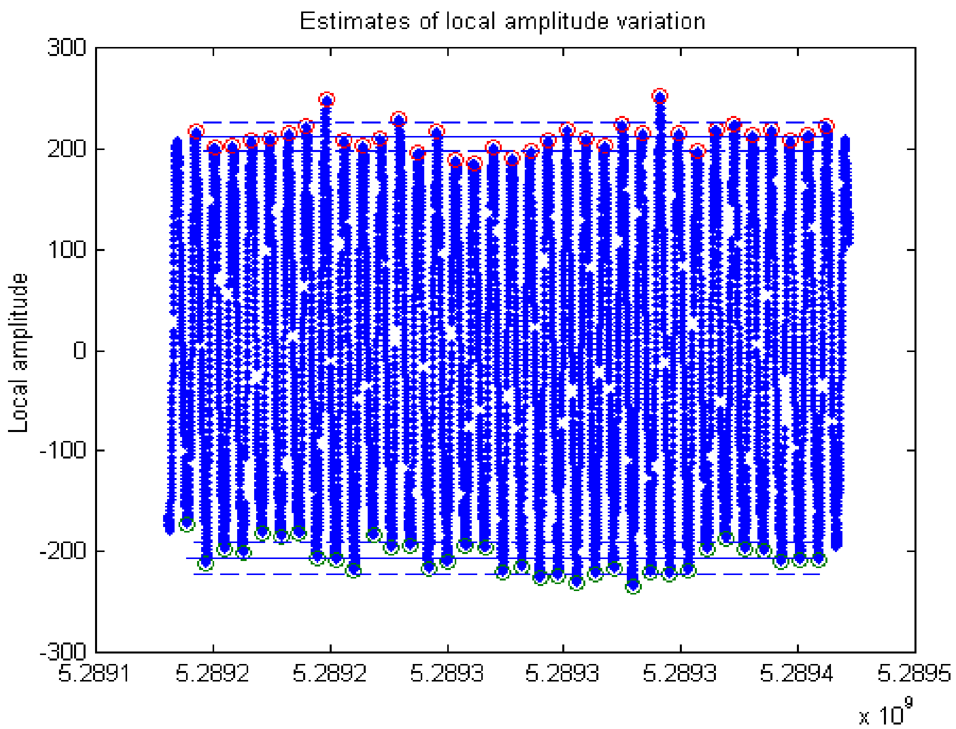

Figure 9. Positions of peaks and troughs (circles), together with the mean and mean ± one standard deviation value (horizontal lines) for data set **a1pf14** (8 µm period grating)

25 µm period grating

Figures 10 and 11 show the two measurement data sets corresponding to the 25 µm period grating corrected for a *linear* misalignment effect. For data set **g3nf1**, the correction would appear to be insufficient, probably due to the form of the shim. For data set **g3pr1**, for which the removal of a linear misalignment effect is more successful, we can expect (as for the 0.8 µm period grating) difficulties in obtaining reliable statistics for the local period, local peak and local trough values because of the affect of form error.

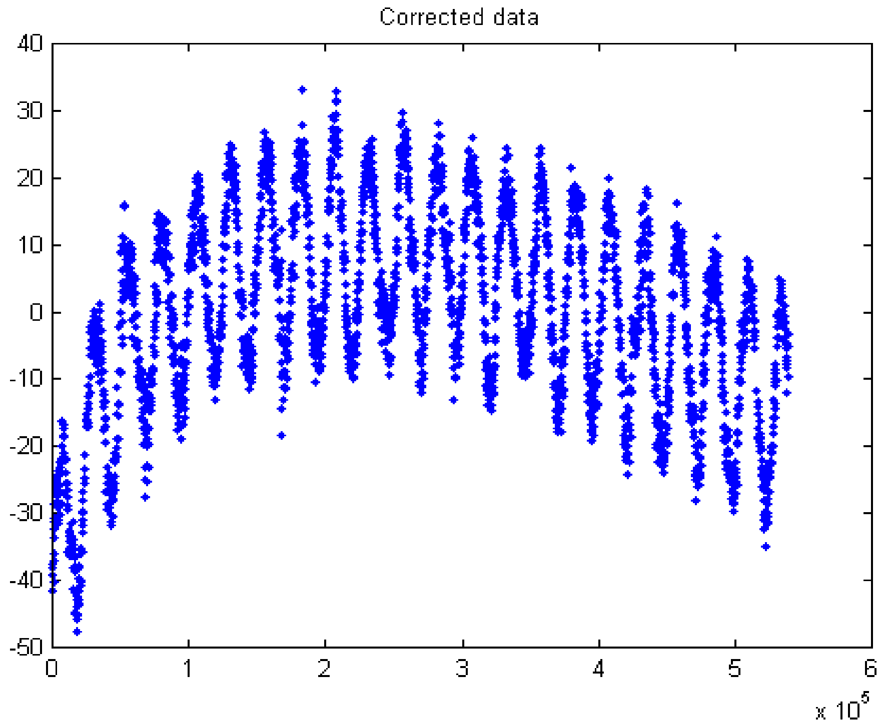

Figure 10. Data set **g3nf1** corrected for linear misalignment (25 µm period grating)

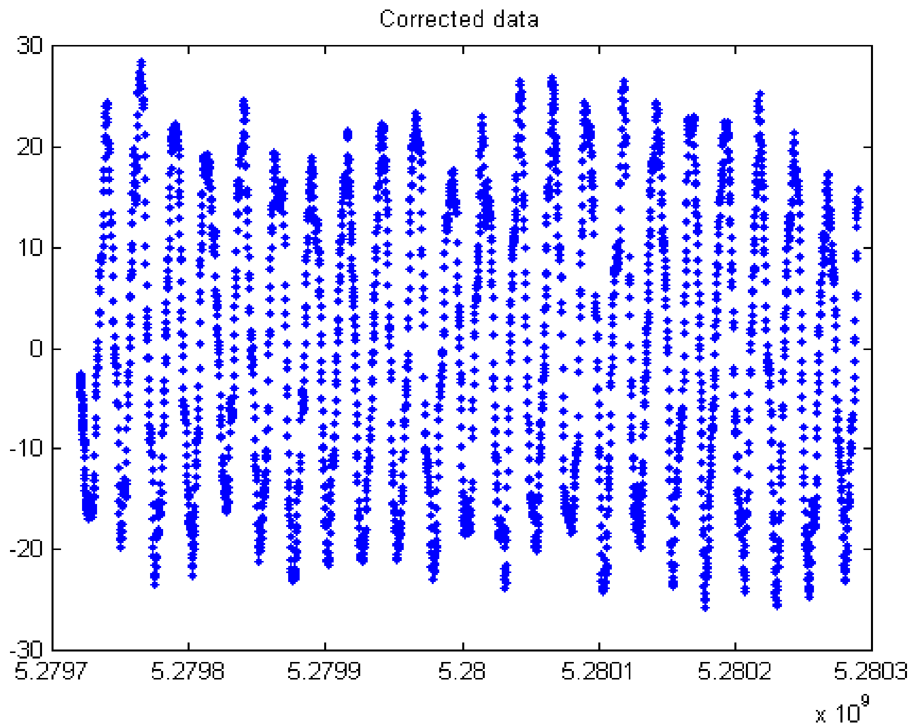

Figure 11. Data set **g3pr1** corrected for linear misalignment (25 µm period grating)

8. REFINEMENT OF THE GRATING GENERATION SYSTEM

Surface irregularities were found to emanate from flaws in the volume of the resist layer. A more stringent substrate cleaning regime was adopted and the photoresist was filtered before spinning to eliminate suspended contaminants.

The aluminised mirror surfaces on the interferometer were cleaned and re-coated in order to remove pinholes, scratches and marks, which were detrimental to the quality of the reflected wavefronts. Mirrors M_2, M_3 and M_4 were re-aluminised using a vacuum evaporation plant. It was decided to replace the 8 inch collimating mirror M_1 with a superior 6 inch one - this was also cleaned and re-aluminised.

Adjustments were made to the interferometer mirrors and beam splitter to reduce and equalise the beam paths. This improved the fringe contrast and reduced any unwanted air turbulence effects. The entire interferometer was boxed-in, to reduce any ambient air turbulence. Before any exposure the substrate was allowed several minutes to thermally stabilise.

The collimation and coherence scrambling optics were mounted in a way that allowed their replacement without altering their relative positions.

Care was taken to ensure constant beam height was maintained above the optical bench in an effort to improve the modulation uniformity.
Modifications were made and systems put in place to facilitate a more systematic approach to the set up and alignment of the interferometer. This improved the repeatability of experiments.

The kinematic substrate holder at the recording plane was mounted on a translation stage - this allowed the substrate to be moved with precision, perpendicular to the bisector of the converging beams. Adjustments to the period of the modulated surfaces can now be made with far less iteration.

9. SECOND GENERATION SINUSOIDS

0.8 μm period grating

Data Set	*Local Period*		*Local Peak*		*Local Trough*	
	Mean (μm)	Standard Deviation (μm)	Mean (nm)	Standard Deviation (nm)	Mean (nm)	Standard Deviation (nm)
800neg1	0.809	0.029	–	–	–	–
800neg2	0.796	0.050	–	–	–	–
800neg3	0.796	0.025	–	–	–	–
800neg4	0.791	0.052	–	–	–	–
800neg5	0.811	0.038	–	–	–	–
800pos1	0.778	0.042	–	–	–	–
800pos2	0.811	0.036	–	–	–	–
800pos3	0.773	0.041	–	–	–	–
800pos4	0.796	0.046	–	–	–	–
800pos5	0.795	0.043	–	–	–	–

In the table above, the mean and standard deviation of the estimates for each grating are given. Figures 12 and 13 show the raw data (after a misalignment correction) with estimates of the peak and trough positions marked.

As for the analysis of the first generation sinusoids of this nominal period (Section 7) the non-parametric analysis of the traces gives spurious values for the local period, and spurious local peaks and troughs are identified. The computed statistics for the variation in local period across each grating are consequently dependent on the scheme used to exclude these spurious values (see Section 6). Statistics relating to local peak and trough values are not reliable and are not presented in the above table.

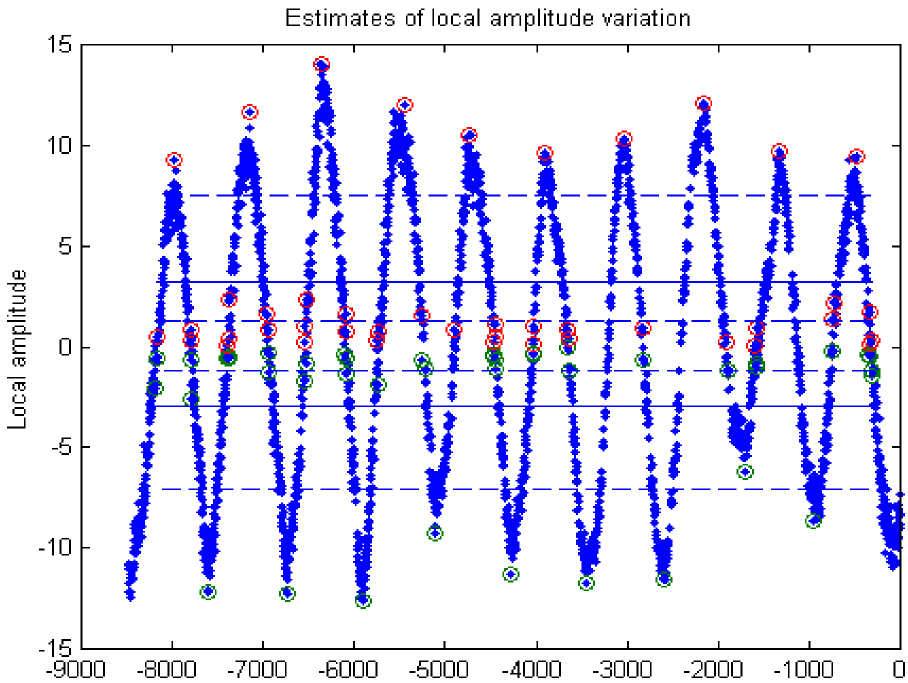

Figure 12. Positions of peaks and troughs (circles), together with the mean and mean ± one standard deviation value (horizontal lines) for data set **800neg1** (0.8 μm period grating)

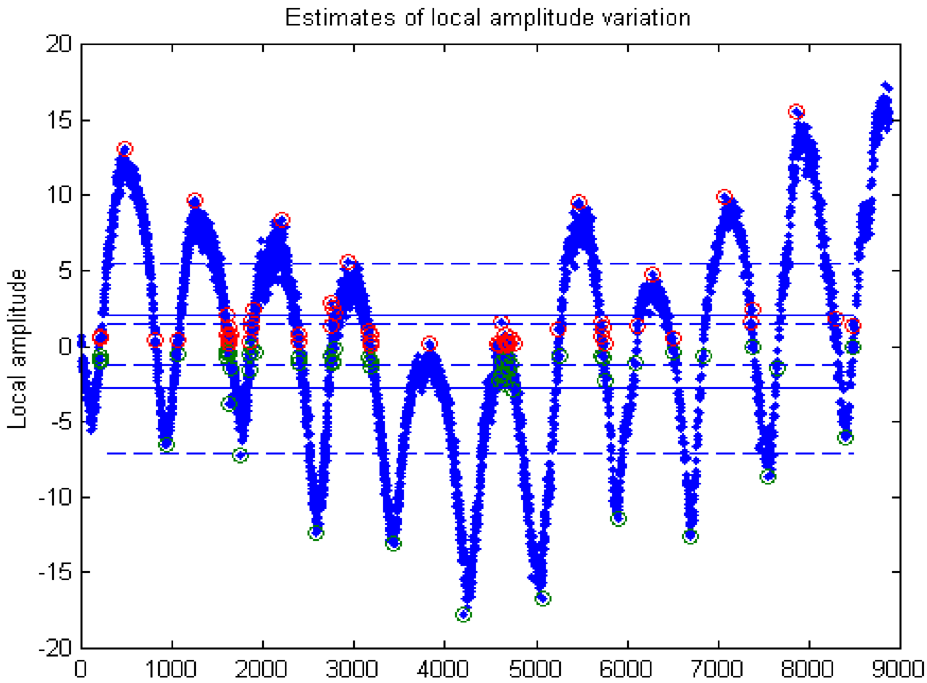

Figure 13. Positions of peaks and troughs (circles), together with the mean and mean ± one standard deviation value (horizontal lines) for data set **800pos1** (0.8 μm period grating)

2.5 μm period grating

Data set	***Local Period***		***Local Peak***		***Local Trough***	
	Mean (μm)	Standard Deviation (μm)	Mean (nm)	Standard Deviation (nm)	Mean (nm)	Standard Deviation (nm)
250neg1	2.543	0.026	-60.982	1.806	54.680	2.564
250neg2	2.545	0.016	-63.361	2.184	59.054	1.844
250neg3	2.542	0.022	–	–	–	–
250neg4	2.541	0.025	–	–	–	–
250neg5	2.542	0.020	-62.913	4.391	54.788	2.218
250pos1	2.530	0.066	-62.357	7.583	50.085	9.145
250pos2	2.542	0.022	-64.885	3.837	50.679	2.499
250pos3	2.543	0.022	-66.557	1.349	50.158	1.642
250pos4	2.541	0.026	–	–	–	–
250pos5	2.543	0.020	–	–	–	–

Figures 14 and 15 show the results of the analysis of the 2.5 μm period gratings, and the table above gives the mean and standard deviation of the estimates of local period, local peak value and local trough value for the gratings. In cases where spurious peaks and troughs are identified in the analysis, statistics relating to local peak and trough values are omitted.

Note that (a) the values of the mean local period for the data sets are very close and exceed the nominal 2.5 μm value, and (b) the traces represented by the data sets have consistent peak-to-valley values.

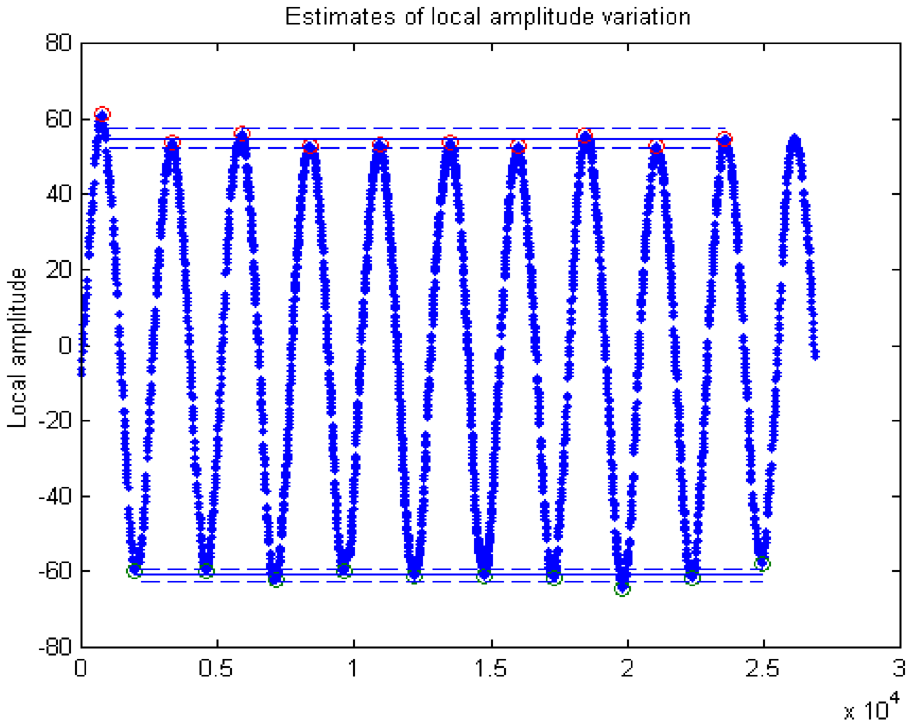

Figure 14. Positions of peaks and troughs (circles), together with the mean and mean ± one standard deviation value (horizontal lines) for data set **250neg1** (2.5 μm period grating)

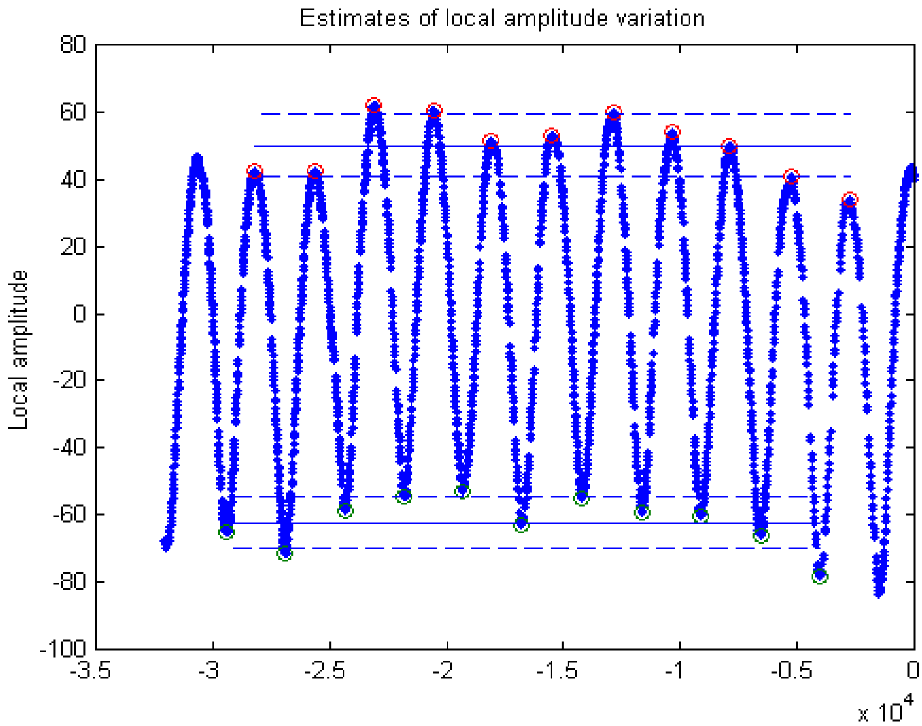

Figure 15. Positions of peaks and troughs (circles), together with the mean and mean ± one standard deviation value (horizontal lines) for data set **250pos1** (2.5 μm period grating)

8 μm period grating

Data set	*Local Period*		*Local Peak*		*Local Trough*	
	Mean (μm)	Standard Deviation (μm)	Mean (nm)	Standard Deviation (nm)	Mean (nm)	Standard Deviation (nm)
8000pos1	7.784	0.197	–	–	–	–
8000pos2	7.739	0.044	−107.672	2.932	92.734	3.819
8000pos3	7.739	0.047	–	–	–	–
8000pos4	7.736	0.047	−110.324	2.743	90.844	3.669
8000pos5	7.738	0.055	–	–	–	–
8000neg1	7.742	0.045	–	–	–	–
8000neg2	7.749	0.043	–	–	–	–
8000neg3	7.752	0.048	–	–	–	–
8000neg4	7.750	0.049	−98.019	1.196	103.961	1.775
8000neg5	7.743	0.054	–	–	–	–

Figures 16 and 17 show the results of the analysis of the 8 μm period gratings, and the table above gives the mean and standard deviation of the estimates of local period, local peak value and local trough value for the gratings.

We note that (a) the values of the mean local period for the data sets are very close and are smaller than the nominal 8 μm value, and (b) the traces represented by the data sets have consistent peak-to-valley values.

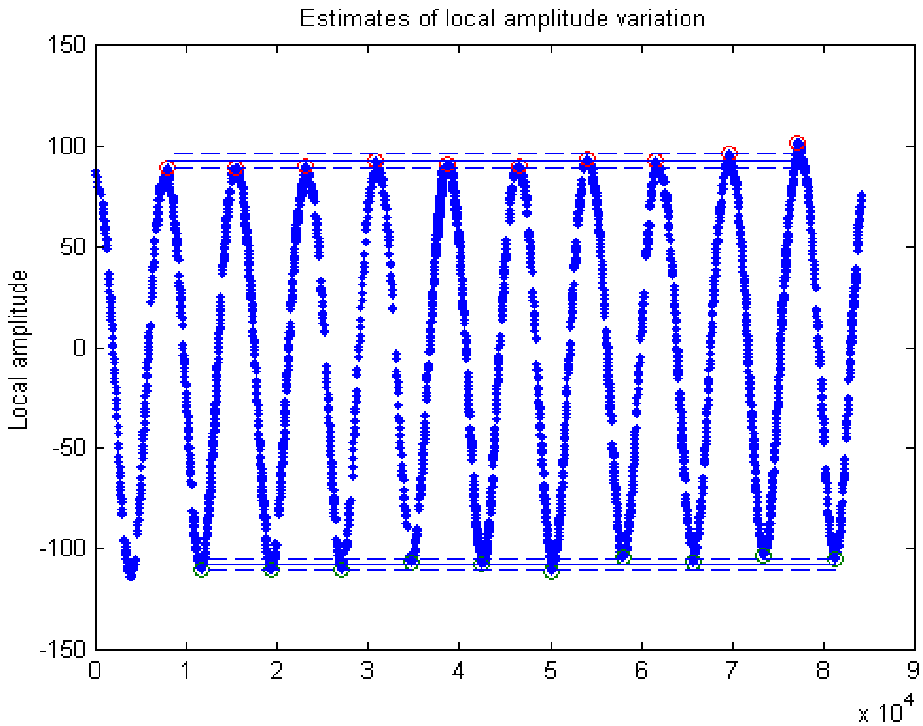

Figure 16. Positions of peaks and troughs (circles), together with the mean and mean ± one standard deviation value (horizontal lines) for data set **8000pos2** (8 μm period grating)

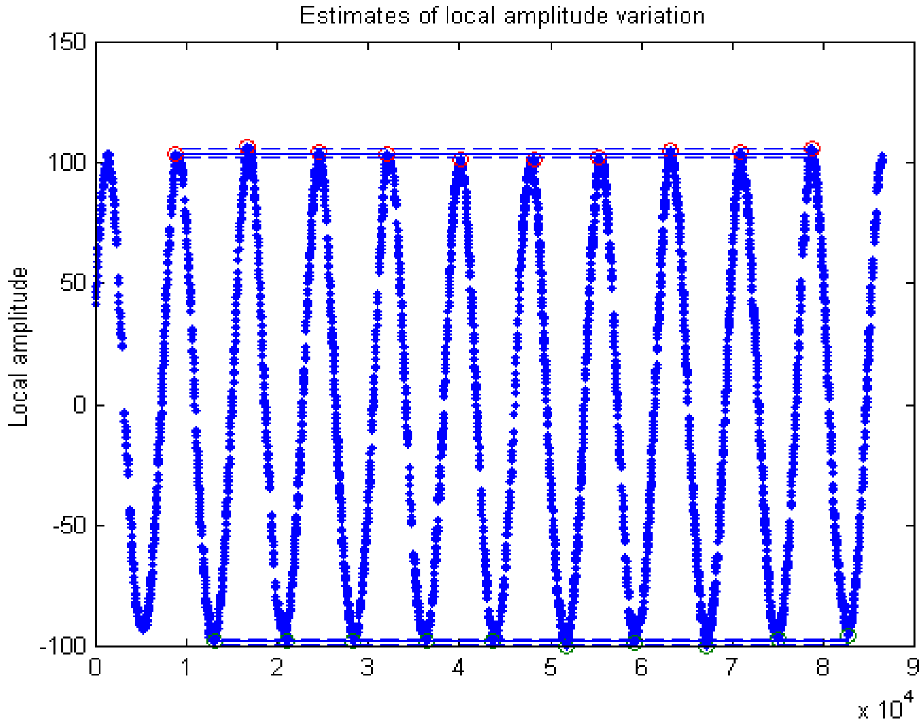

Figure 17. Positions of peaks and troughs (circles), together with the mean and mean ± one standard deviation value (horizontal lines) for data set **8000neg4** (8 μm period grating)

25 μm period grating

Data set	***Local Period***		***Local Peak***		***Local Trough***	
	Mean (μm)	Standard Deviation (μm)	Mean (nm)	Standard Deviation (nm)	Mean (nm)	Standard Deviation (nm)
2500neg1	25.209	0.048	−555.654	14.979	507.988	15.358
2500neg2	25.211	0.035	−535.868	7.832	514.893	10.027
2500neg3	25.215	0.056	−549.113	17.241	507.038	17.100
2500neg4	25.209	0.029	−550.932	7.319	531.078	5.885
2500neg5	25.209	0.029	−550.932	7.319	531.078	5.885
2500pos1	25.215	0.028	−532.347	4.473	544.821	5.400
2500pos2	25.223	0.085	−532.186	24.602	542.134	23.321
2500pos3	25.220	0.074	−518.572	18.941	540.803	21.165
2500pos4	25.210	0.024	−545.237	1.890	543.107	3.533
2500pos5	25.209	0.054	−545.511	15.837	555.704	15.908

Figures 18 and 19 show the results of the analysis of the 25 μm period gratings, and the table above gives the mean and standard deviation of the estimates of local period, local peak value and local trough value for the gratings. In all cases the local peaks and troughs are correctly identified by the analysis scheme, and so a complete set of statistics is presented in the table.

We note that (a) the values of the mean local period for the data sets are very close and exceed the nominal 25 μm value, and (b) in some cases there is a linear variation in the local peak and local trough values across the grating. The second generation sinusoid gratings considered here would appear to be much better characterised than the first generation sinusoids considered in Section 7.

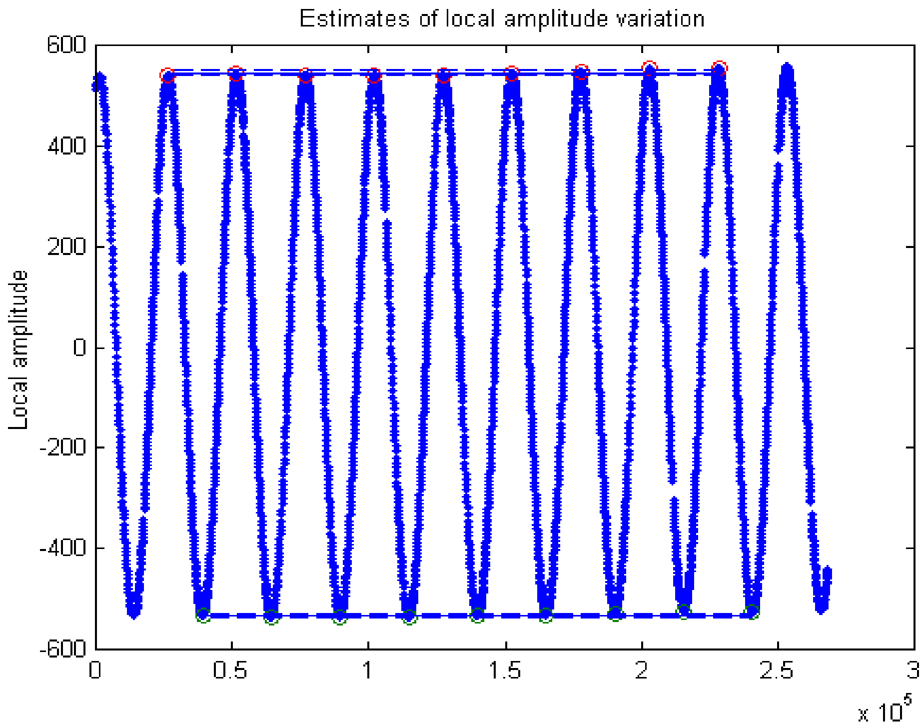

Figure 18. Positions of peaks and troughs (circles), together with the mean and mean ± one standard deviation value (horizontal lines) for data set **2500pos1** (25 µm period grating)

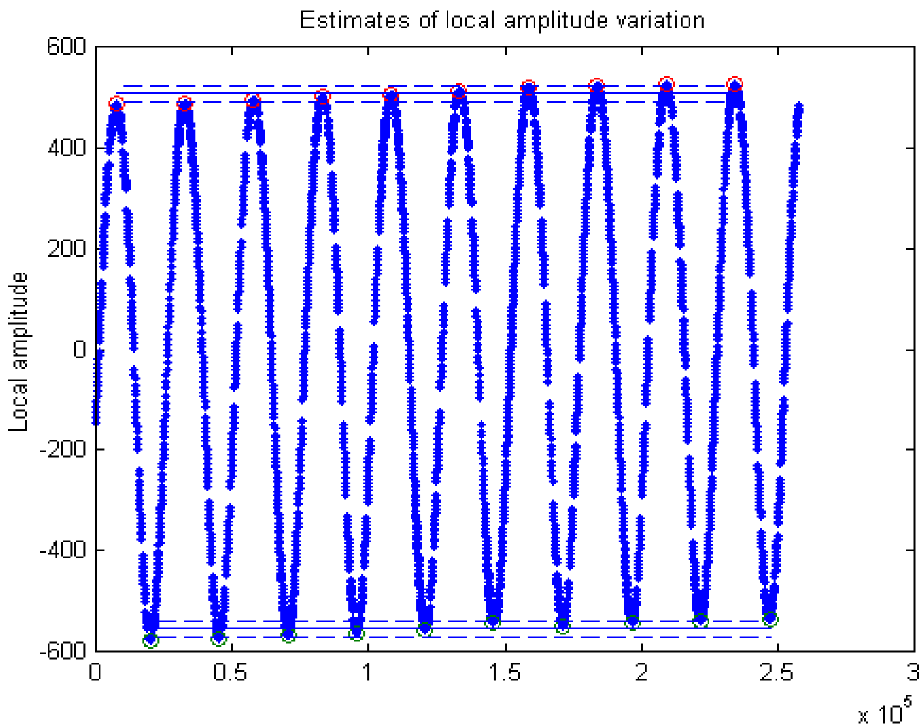

Figure 19. Positions of peaks and troughs (circles), together with the mean and mean ± one standard deviation value (horizontal lines) for data set **2500neg1** (25 µm period grating)

10. CONCLUSIONS

From the results it is clear that, with exception of the 0.8 μm period gratings, the second generation of gratings are of a much better quality than their predecessors. There is evidence of a strong interaction of the stylus with the 0.8 μm grating, but it was not considered worthwhile measuring these gratings using the NPL Metrological AFM (Leach, Haycocks, *et. al.* 2000) because their overall quality would rule them out for use as Type C1 standards. The methods employed by NPL in this project are not considered appropriate for gratings with periods of less than 2.5 μm. However, gratings such as those with 8 and 25 μm periods have been produced that would be extremely useful as Type C1 calibration artefacts for surface texture measuring instruments.

11. ACKNOWLEDGEMENTS

The authors would like to thank Dr Mike Hutley and Mr Nick Turner for early contributions to the project. Thanks also to Mrs Anne Hart who carried the measurements using NanoSurf IV. The work was funded by the EC under project number SMT4 – CT97 – 2176.

12. REFERENCES

PD 6461: Part 3: 1995 *Vocabulary of metrology Part 3. Guide to the expression of uncertainty in measurement,* International Organization for Standardization (ISO), Switzerland

ISO 5436: 1999 *Geometrical product specifications (GPS) – Surface texture: Profile method; Measurement standards* (International Organization for Standardization)

Leach R K 1999 Calibration, traceability and uncertainty issues in surface texture metrology *NPL Report* **CLM 7** 1-56

Leach R K 2000 Traceable measurement of surface texture at the National Physical Laboratory using NanoSurf IV *Meas. Sci. Technol.* **11** 1162-1172

Leach R K, Haycocks J, Jackson K, Lewis A J, Oldfield S, Yacoot A 2000 Advances in traceable nanometrology at the National Physical Laboratory *Proc. future directions in nanotechnology in Europe and Japan, 18th-21st Sept., Warwick* pp112-128